Phys. Status Solidi B **252,** No. 11, 2380–2384 (2015) / **DOI** 10.1002/pssb.201552224

physica status solidi b
www.pss-b.com
basic solid state physics

Invited Article

Stokes and anti-Stokes Raman spectra of the high-energy C–C stretching modes in graphene and diamond

Ado Jorio[*,1], Mark Kasperczyk[2], Nick Clark[3], Elke Neu[,4], Patrick Maletinsky[**,4], Aravind Vijayaraghavan[3], and Lukas Novotny[2]**

[1] Departamento de Física, Universidade Federal de Minas Gerais, Belo Horizonte, MG 31270-901, Brazil
[2] Photonics Laboratory, ETH Zürich, 8093 Zürich, Switzerland
[3] School of Materials and National Graphene Institute, University of Manchester, Manchester M13 9PL, United Kingdom
[4] Department of Physics, University of Basel, Klingelbergstrasse 82, 4056 Basel, Switzerland

Received 17 April 2015, revised 8 August 2015, accepted 11 August 2015
Published online 4 September 2015

Keywords anti-Stokes scattering, diamond, graphene, Raman spectroscopy

[*] Corresponding author: e-mail adojorio@fisica.ufmg.br, Phone: +55 31 34096610, Fax: +55 31 34095600
[**] Present address: Universität des Saarlandes, Experimentalphysik Building E2.6, Office 1.17, 66123 Saarbrücken, Germany.

The Stokes and the anti-Stokes Raman spectra from the high energy carbon–carbon stretching modes in graphene and diamond are studied, with a focus on their intensity dependence on the excitation laser power. For diamond, the experiment was performed on a 50 μm slice of chemical vapour deposition grown single crystal using a 785 nm laser, in both the continuous wave (CW) and pulsed mode-locked (ML—130 fs pulses) excitation regimes. For graphene, the experiments were performed on suspended samples, including single layer, bilayer with AB-staking, twisted bi-layer and a sample with 4–6 layers, using $\lambda = 532$ and 633 nm CW lasers. The Stokes and anti-Stokes intensities vary largely from sample to sample, and the anti-Stokes/Stokes intensity ratio shows different excitation laser power behaviours. These differences can be explained on the basis of laser heating or correlated Stokes–anti-Stokes scattering phenomena.

1 Introduction Phonons are quantum states of the harmonic oscillators, having their increase and decrease in number n described by the creation ($a^\dagger$) and annihilation (a) operators. The action of these operators on an eigenstate $|n\rangle$ introduces normalisation factors given by $a^\dagger|n\rangle = (n+1)^{1/2}|n+1\rangle$ and $a|n\rangle = n^{1/2}|n-1\rangle$. In the inelastic scattering of light by phonons, a photon creates or annihilates a phonon, in the so-called Stokes or anti-Stokes Raman scattering processes. The intensity ratio between the Stokes and anti-Stokes components (I_{aS}/I_S) is, therefore, usually determined by the quantum mechanical normalisation factors, $I_{aS}/I_S \propto n/(n+1)$ [1, 2].

The thermal population of phonons is given by the Bose–Einstein distribution function $n_0 = [\exp(E_q/k_BT) - 1]^{-1}$, where E_q and k_BT are the phonon and thermal energies, respectively. Replacing n by n_0 in the anti-Stokes/Stokes intensity ratio gives $I_{aS}/I_S = C(n_0+1)/n_0 = C\exp(E_q/k_BT)$, where C is a constant that comprehends all the optical parameters. This equation can be inverted to obtain the effective phonon temperature in a material by measuring their Stokes and anti-Stokes Raman spectra, given by $T = E_q/\{k_B[\ln C - \ln(I_{aS}/I_S)]\}$. This procedure has been largely used in the literature to study the phonon population dependence of different nanomaterials properties, including electrical power [3], thermal conductivity [4], effective temperatures on biased nanostructures [5], phonon anarmonicities and lifetimes [6, 7] and optical transitions [8, 9]. Generally, the constant C is found by setting T to room temperature for very low laser power (or zero bias), where sample heating should not be present.

One aspect that is not considered in this type of treatment is the possibility that one single phonon that is created in the Stokes process is subsequently annihilated in the anti-Stokes process. This correlated Stokes-anti-Stokes scattering (SaS) phenomenon was proposed in 1977 by Klyshko [10], and it has been shown to affect the anti-Stokes and Stokes intensities in graphene [11] and diamond [12, 13]. A theoretical framework to address this phenomenon

has been proposed, demonstrating implications for the anti-Stokes/Stokes intensity ratio [14].

In this article we will explore the laser power dependence for diamond and graphene, including the dependence on the layer stacking, on different excitation laser energies, and on the difference between a continuous wave (CW) laser or a pulsed mode-locked (ML) laser regime. Some of the results shown here have already been discussed in Refs. [11, 13, 14], but here we present a deeper comparative analysis. The differences can be explained on the basis of laser heating or correlated SaS phenomena.

2 Methods

2.1 Samples Graphene and diamond samples are studied here. Graphene has a first-order Raman allowed peak at 1584 cm^{-1}, named G band. Diamond has a first-order Raman allowed peak at 1332 cm^{-1}. In both cases, these Raman bands are related to the C–C stretching modes.

The diamond sample was grown by the chemical vapour deposition (CVD) method, with cutting and polishing generating a highly pure free-standing 50 μm thick diamond crystal [13]. As for the graphene samples, Fig. 1 shows an optical image. The graphene sample has been deposited on top of a SiN_x substrate with holes. The graphene flakes are suspended over the holes, and the light can pass through the graphene sample without touching the substrate. More details can be found in Ref. [11]. Four types of graphene samples were studied: single-layer graphene, double-layer graphene with AB-stacking, twisted bilayer graphene (tBLG) and a 4–6 layers graphene with AB-stacking. All the samples were prepared by mechanical exfoliation of graphite, and deposited on a similar substrate, as shown in Fig. 1. The tBLG [15] was engineered to exhibit a twist angle $\theta = 11^\circ$, which generates a peak in the joint density of states that lies between the common laser wavelengths of 633 and 532 nm [11]. In this way, when exciting the tBLG with a 633 nm laser, the G band anti-Stokes Raman emission is resonant. When exciting the tBLG sample with the 532 nm laser, the G band Stokes Raman emission is resonant.

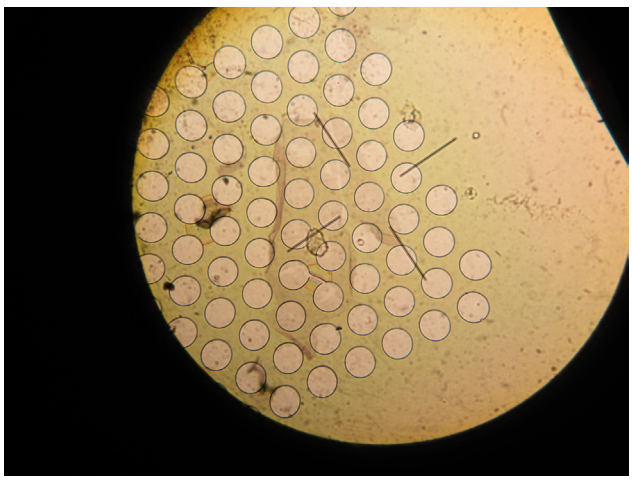

Figure 1 Optical image of the graphene sample. The holes in the SiN_x substrate are 10 μm in diameter.

2.2 Experimental details The graphene samples were excited with a frequency doubled Nd:YVO_4 laser at $E_{laser} = 2.33$ eV ($\lambda_{laser} = 532.0$ nm) and with a HeNe laser at $E_{laser} = 1.96$ eV ($\lambda_{laser} = 632.8$ nm), both working in the CW regime. As already specified, these two lasers are off resonance with respect to the peak in the joint density of states (JDOS) for the tBLG, E_{laser} being blue- or red-shifted from the JDOS peak by approximately the G band phonon energy ($E_G = 0.2$ eV) [11]. The signal was collected through a spectrometer, equipped with a charge coupled device (CCD) detector and filtered using optical notches and band pass filters.

The diamond sample was studied with a Ti:Sapph laser at $\lambda = 785$ nm, which can work both in the CW (continuous wave) and ML (mode locked–pulsed) regimes. For ML, the duration of the excitation laser pulses is $\tau = 130$ fs, with a repetition rate of $\Delta f = 76$ MHz.

Finally, a 200 fs pulsed laser at $\lambda = 545$ nm from an OPO was used to excite both diamond and one of the graphene samples, for comparative analysis.

3 Results and discussions

3.1 Pulsed laser Raman spectra Figure 2 shows the Stokes and anti-Stokes Raman spectra of the 4–6 layers graphene and diamond samples, obtained with a 200 fs pulsed laser at $\lambda = 545$ nm, with average excitation laser power $P_{laser} = 20$ mW. For diamond (the dark green line),

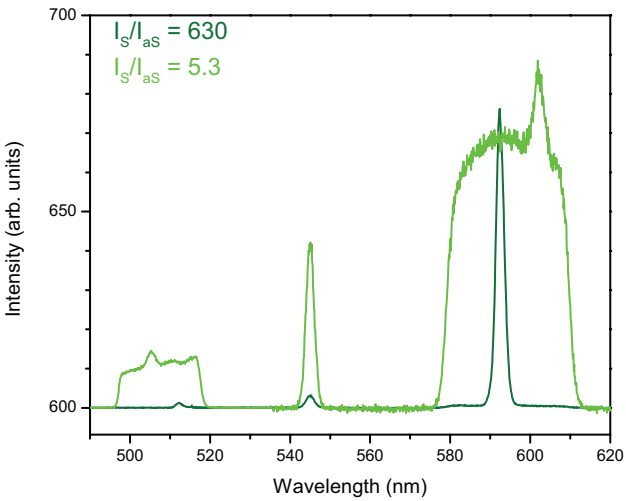

Figure 2 Stokes and anti-Stokes Raman spectra of graphene (light green) and diamond (dark green) obtained with a 200 fs pulsed laser at $\lambda = 545$ nm. The Stokes/anti-Stokes intensity ratio (I_S/I_{aS}) is also displayed for both samples, following the same colour code. The 1332 cm^{-1} diamond peaks appear at 592 and 512 nm for the Stokes and anti-Stokes scattering, respectively. The 1584 cm^{-1} graphene peaks appear at 602 and 505 nm for the Stokes and anti-Stokes scattering, respectively.

the central peak at $\lambda = 545$ nm is leakage from the laser, and the peaks at 512 and 592 nm are the anti-Stokes and Stokes Raman peaks, respectively. The width of the peaks is determined by the spectral width of the 200 fs laser pulses.

For graphene (light green in Fig. 2), again the peak at $\lambda = 545$ nm is leakage from the laser, whereas the anti-Stokes and Stokes Raman peaks appear at wavelengths (505 and 602 nm, respectively), which are different from those in diamond, as the phonon energy is different. To measure the Raman signals, we used a band-pass filter at (506 ± 20) nm for the anti-Stokes signal, and a band-pass filter at (600 ± 20) nm for the Stokes signal. The square-shaped signals observed within these ranges in Fig. 2 come from the hot luminescence of graphene, which appears when graphene is excited with pulsed lasers [16].

Analysing the Raman peak intensities with a single Lorentizan fit, we found the Stokes/anti-Stokes intensity ratio for diamond $I_S/I_{aS} = 630$, which is close to the expected value for the diamond phonon ($1332\,cm^{-1}$), in agreement with the Bose–Einstein phonon population at room temperature ($T = 295$ K). For the graphene sample (G band at $1584\,cm^{-1}$), the Stokes/anti-Stokes intensity ratio is $I_S/I_{aS} = 5.3$, which is three orders of magnitude smaller than the expected value from the Bose–Einstein phonon population at room temperature. This result indicates that either the graphene sample exhibits a very high laser-induced phonon temperature, or that the Stokes-anti-Stokes correlated scattering phenomenon is the dominating process. Correlation measurements, as performed in Refs. [12, 13] are not possible here due to the strong hot luminescence [16].

3.2 Spectral power dependence Figure 3 shows the excitation laser power dependence for the Stokes and anti-Stokes intensities normalised by the excitation laser power, from all the samples studied in this work. Green, red and black/grey symbols indicate Raman spectra obtained with the lasers at $\lambda_{laser} = 532.0$, 632.8 and 785, respectively. The different symbol shapes indicate the specific samples, as displayed in the figure legend. Graphene data were obtained with CW lasers. Filled and opened symbols stand for Stokes and anti-Stokes intensities, respectively, except for diamond excited by the CW laser, for which the spheres represent both Stokes and anti-Stokes intensities.

In Fig. 3, the laser-power normalised Stokes intensities (filled symbols) show a constant value, in agreement with a linear dependence of I_S on the excitation laser power. The laser-power normalised anti-Stokes intensities exhibit a super-linear power dependence. Therefore, the anti-Stokes responses demonstrate that either laser-induced heating or correlated SaS are taking place.

Figure 4 shows more clearly the behaviour of the diamond Raman responses. For CW excitation, both Stokes (black spheres) and anti-Stokes (grey spheres) exhibit a linear dependence with the excitation laser power, which is evident in Fig. 4 by a constant value for "Intensity/Laser

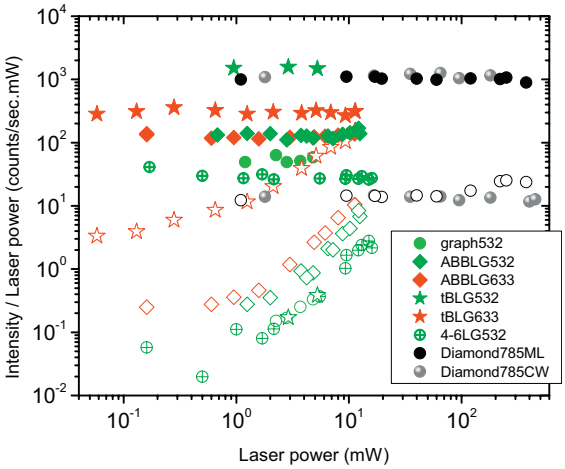

Figure 3 Laser power dependence for the power-normalized Stokes and anti-Stokes scattering intensities for diamond and different graphene samples. The different samples are indicated by different symbols, according to the legend: graph 532 – single layer graphene excited with $\lambda = 532$ nm; ABBLG532 – AB-stacked bilayer graphene excited with $\lambda = 532$ nm; ABBLG633 – AB-stacked bilayer graphene excited with $\lambda = 633$ nm; tBLG532 – twisted bilayer graphene excited with $\lambda = 532$ nm; tBLG633 – twisted bilayer graphene excited with $\lambda = 633$ nm; 4-6LG532 – 4 to 6-layers graphene with AB-stacking excited with $\lambda = 532$ nm (graphene data were obtained with CW lasers); Diamond785ML – diamond excited with $\lambda = 785$ nm in the pulsed mode locked regime; Diamond785CW – diamond excited with $\lambda = 785$ nm in the continuous wave regime.

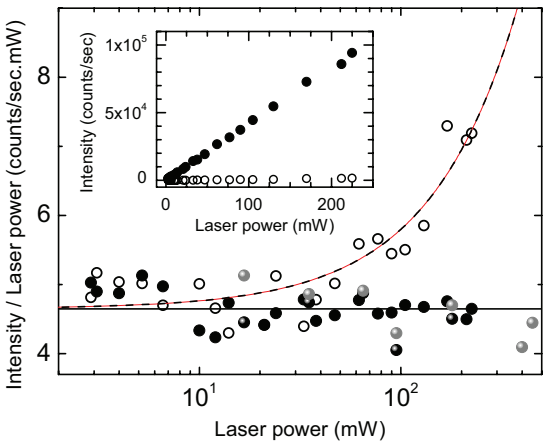

Figure 4 Excitation laser power dependence for the Stokes and anti-Stokes Raman intensities for diamond, normalized (i) by the laser power and (ii) by a constant factor to merge the Stokes and anti-Stokes intensities. Black and grey spheres stand for Stokes and anti-Stokes Raman intensities obtained in the CW excitation regime. Filled and open circles stand for the Stokes and anti-Stokes Raman intensities obtained in the pulsed ML excitation regime. For the spectra obtained in the ML pulsed regime, laser power denotes the average laser power, and not the peak laser power. The inset shows the non-normalized Stokes and anti-Stokes intensities as measured in the pulsed ML regime, on a linear scale.

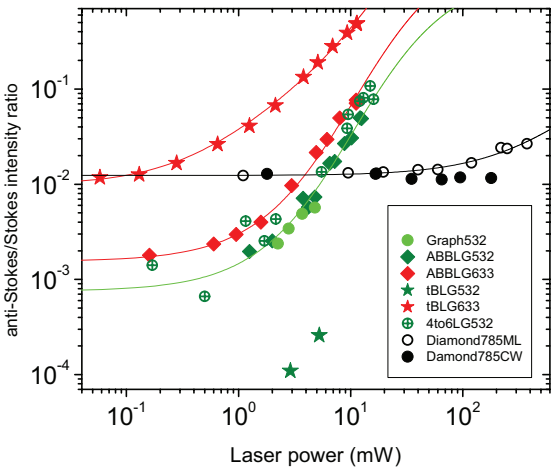

Figure 5 Excitation laser power dependence for the anti-Stokes/Stokes Raman intensity ratio (I_{aS}/I_S) for diamond (black data) and for the different graphene samples (green and red data). Sample specification is found in the figure legend: Graph 532 – single layer graphene excited with $\lambda = 532$ nm; ABBLG532 – AB-stacked bilayer graphene excited with $\lambda = 532$ nm; ABBLG633 – AB-stacked bilayer graphene excited with $\lambda = 633$ nm; tBLG532 – twisted bilayer graphene excited with $\lambda = 532$ nm; tBLG633 – twisted bilayer graphene excited with $\lambda = 633$ nm; 4to6LG532 – 4 to 6-layers graphene with AB-stacking excited with $\lambda = 532$ nm; Diamond785ML – diamond excited with $\lambda = 785$ nm in the pulsed mode locked regime; Diamond785CW – diamond excited with $\lambda = 785$ nm in the continuous wave regime. The lines are fitting curves to the data according to the theory presented in Ref. [14].

power". For the ML pulsed excitation, the Stokes signal (black circles) shows a linear dependence on the excitation laser power, evidenced by a constant "Intensity/Laser power" in Fig. 4, whereas the anti-Stokes signal (open circles) shows a super-linear dependence.

3.3 Anti-Stokes/Stokes intensity ratio Figure 5 shows the excitation power dependence behaviour for the I_{aS}/I_S intensity ratio for all the samples studied in this work.

For diamond, I_{aS}/I_S is constant for the CW excitation (black circles). This indicates that neither heating nor the correlated SaS are relevant [17]. However, for the pulsed ML excitation, the behaviour is super-linear. It has been shown already that this super-linear behaviour is due to the correlated SaS scattering [12–14]. As the SaS is a non-linear process, the ultra-high intensities within a laser pulse are needed to produce the effect in diamond.

For graphene, a difference in behaviour is observed when comparing the tBLG in resonance with the anti-Stokes photon emission (red star data) and all the other samples. The data are fit with the theory introduced in Ref. [14]. The excitation laser power dependences for single layer graphene (light green circle), AB-stacked bilayer graphene (diamond symbols), and 4–6-layers graphene (crossed circles) indicate an I_{aS}/I_S dependence dominated by thermal effects. The excitation laser power dependence for twisted bilayer graphene in resonance with the anti-Stokes photon emission (red star data) indicates an I_{aS}/I_S dependence dominated by the SaS correlated scattering, consistent with Ref. [14]. For tBLG in resonance with the Stokes photon emission (green star data), only two data points are obtained due to the very low anti-Stokes intensity, which is not enough for a fitting analysis. For graphene, all the spectra were obtained in the CW excitation regime.

When comparing graphene and diamond, the first important difference is the phonon energy, which influences the Bose–Einstein distribution. Additionally, diamond is transparent for visible and lower light energies, whereas graphene is always in resonance with the light absorption and emission. The SaS phenomenon appears here in diamond when ultra-high intensities from a pulsed laser is in place, whereas the specially engineered tBLG shows the phenomenon at much lower average powers, even for a CW laser. More work is needed to characterise the SaS process in graphene, especially because the strong hot luminescence prevents the use of pulsed lasers for photon coincidence experiments.

4 Conclusions In this work, we measured the power dependence of the Stokes and anti-Stokes intensities from a 50 μm thick diamond crystal and from different graphene samples, including single-layer, bilayer and 4–6-layers graphenes. The I_{aS}/I_S intensity ratio varies from sample to sample, and it also depends on the excitation conditions (pulsed vs. continuous wave). The results are analysed considering two distinct effects, namely laser induced heating and the production of correlated Stokes–anti-Stokes photon pairs.

Our results indicate that there is no heating in diamond. For CW laser excitation, this is proven by a constant value of the I_{aS}/I_S ratio. For the pulsed laser excitation, the increase in the I_{aS}/I_S ratio comes from the correlated Stokes–anti-Stokes scattering. For graphene, the correlated Stokes–anti-Stokes scattering is dominant for tBLG when in resonance with the scattered anti-Stokes emission. Otherwise, heating is the dominant phenomenon.

Acknowledgements A.J. acknowledges CAPES and ETH for financing his visit to ETH Zurich, and CNPq grant 460045/2014-8. L.N. thanks financial support by the Swiss National Science Foundation (SNF) through grant 200021-14 6358. A.V. thanks the Engineering and Physical Sciences Research Council (EPSRC) for financial support through Grants EP/G035954/1 and EP/K009451/1.

References

[1] C. V. Raman and K. S. Krishnan, Nature **121**, 501 (1928).
[2] A. Jorio, M. S. Dresselhaus, and R. Saito, Raman Spectroscopy in Graphene Related Systems (Wiley-VCH, Weinheim, 2011).
[3] M. Steiner, M. Freitag, V. Perebeinos, J. C. Tsang, J. P. Small, M. Kinoshita, D. Yuan, J. Liu, and P. Avouris, Nature Nanotechnol. **4**, 320 (2009).

[4] C. Faugeras, B. Faugeras, M. Orlita, M. Potemski, R. R. Nair, and A. K. Geim, ACS Nano **4**, 1889 (2010).
[5] S. Berciaud, M. Y. Han, K. F. Mak, L. E. Brus, P. Kim, and T. F. Heinz, Phys. Rev. Lett. **104**, 227401 (2010).
[6] N. Bonini, M. Lazzeri, N. Marzari, and F. Mauri, Phys. Rev. Lett. **99**, 176802 (2007).
[7] D. Song, F. Wang, G. Dukovic, M. Zheng, E. D. Semke, L. E. Brus, and T. F. Heinz, Phys. Rev. Lett. **100**, 225503 (2008).
[8] A. Jorio, A. G. Souza, Filho, G. Dresselhaus, M. S. Dresselhaus, R. Saito, J. H. Hafner, C. M. Lieber, F. M. Matinaga, M. S. S. Dantas, and M. A. Pimenta, Phys. Rev. B **63**, 245416 (2001).
[9] A. G. Souza, Filho, A. Jorio, J. H. Hafner, C. M. Lieber, R. Saito, M. A. Pimenta, G. Dresselhaus, and M. S. Dresselhaus, Phys. Rev. B **63**, 241404(R) (2001).
[10] D. N. Klyshko, Sov. J. Quantum Electron. **7**, 755 (1977).
[11] A. Jorio, M. Kasperczyk, N. Clark, E. Neu, P. Maletinsky, A. Vijayaraghavan, and L. Novotny, Nano Lett. **14**, 5687 (2014).
[12] K. C. Lee, B. J. Sussman, M. R. Sprague, P. Michelberger, K. F. Reim, J. Nunn, N. K. Langford, P. J. Bustard, D. Jaksch, and I. A. Walmsley, Nature Photon. **6**, 41 (2012).
[13] M. Kasperczyk, A. Jorio, E. Neu, P. Maletinksy, and L. Novotny, Opt. Lett. **40**(10), 2393 (2015).
[14] C. A. Parra-Murillo, M. F. Santos, C. H. Monken, and A. Jorio, arXiv:1503.01518 (2015).
[15] A. Jorio and L. G. Cançado, Solid State Commun. **175**, 3 (2013).
[16] C. H. Lui, K. F. Mak, J. Shan, and T. F. Heinz, Phys. Rev. Lett. **105**, 127404 (2010).
[17] H. Herchen and M. A. Cappelli, Phys. Rev. B **43**, 11740 (1991).

